J. Membrane Biol. 195, 165–182 (2003)
DOI: 10.1007/s00232-003-0617-z

The Journal of
Membrane
Biology

The Kinetics of Non-Lamellar Phase Formation in DOPE-Me: Relevance to Biomembrane Fusion

V. Cherezov[1], D.P. Siegel[1]*, W. Shaw[2], S.W. Burgess[2], M. Caffrey[1]
[1]Biochemistry, Biophysics and Chemistry, The Ohio State University, 100W 18th Ave., Columbus, OH 43210, USA
[2]Avanti Polar Lipids Inc., 700 Industrial Park Dr., Alabaster, AL 35007, USA

Received: 14 May 2003/Accepted: 15 July 2003

Abstract. The mechanism of the lamellar/inverted cubic (Q_{II}) phase transition is related to that of membrane fusion in lipid systems. N-Monomethylated dioleoylphosphatidylethanolamine (DOPE-Me) exhibits this transition and is commonly used to investigate the effects of exogenous substances, such as viral fusion peptides, on the mechanism of membrane fusion. We studied DOPE-Me phase behavior as a first step in evaluating the effects of membrane-spanning peptides on inverted phase formation and membrane fusion. These measurements show that: a) the onset temperatures for Q_{II} and inverted hexagonal (H_{II}) phase formation both are temperature scan rate-dependent; b) longer pre-incubation times at low temperature and lower temperature scan rates favor formation of the Q_{II} phase; and c) in temperature-jump experiments between 61 and 65°C, the metastable H_{II} phase forms initially, and disappears slowly while the Q_{II} phase develops. These observations are rationalized in the context of a mechanism for both the lamellar/non-lamellar phase transition and the related process of membrane fusion.

Key words: Calorimetry — Cubic phase — Fusion mechanism — Hexagonal phase — Lamellar phase — Time-resolved x-ray diffraction

Correspondence to: M. Caffrey, email: caffrey.1@osu.edu

**Current address* for D.P.S.: Givaudan, Cincinnati, OH 45216

Data Deposition: Relevant transition temperatures in this paper have been deposited in the LIPIDAT (http://www.lipidat.chemistry.ohio-state.edu/miscellaneous.htm)

Introduction

N-monomethylated dioleoylphosphatidylethanolamine (DOPE-Me) has been used extensively to study the relationship between membrane fusion and inverted phase formation. Membrane fusion in large unilamellar vesicle (LUV) dispersions of DOPE-Me occurs at the same temperature at which multilamellar vesicles (MLVs) of DOPE-Me in excess water evolve "isotropic" or inverted cubic structures (Ellens et al., 1989; Siegel et al., 1989a). Electron microscopy experiments have shown that the intermediates in membrane fusion in LUV dispersions are also intermediates in lamellar/inverted cubic (L_α/Q_{II}) phase transitions (Ellens et al., 1989; Siegel et al., 1989b; Siegel, Green & Talmon, 1994). Hence, many groups have studied the effects of peptides and lipid additives on membrane fusion, in part, by studying their effects on the evolution of isotropic and inverted cubic phases (Yeagle et al., 1991; Epand & Epand, 1994; Epand et al., 1994; Nieva et al., 1995; Colotto et al., 1996; Colotto & Epand, 1997; Basáñes, Gõni & Alonso, 1998; Davies et al., 1998; Darkes et al., 2002). In several cases, DOPE-Me was the lipid of choice (Yeagle et al., 1991; Epand & Epand, 1994; Epand et al., 1994; Colotto et al., 1996; Colotto & Epand, 1997; Davies et al., 1998; Darkes et al., 2002), since it is one of a few single lipid-component glycerophospholipid systems that forms Q_{II} phases. In multi-component phospholipid systems such as DOPE/DOPC, preferential association of additives with one or the other component, and enrichment of disparate phases with different lipid components, are experimental concerns. In addition, the L_α/Q_{II} phase transition in DOPE-Me is slow (Siegel & Banschbach, 1990), so that increases in the formation rate of isotropic or Q_{II} phases are easy to detect. Such studies, involving the effects of membrane-spanning peptides on Q_{II} phase formation, are underway in our laboratory.

In previous studies of DOPE-Me (Siegel & Banschbach, 1990) it was shown that the lipid can form the Q_{II} phase at slow scan rates or during prolonged incubations. In the process of examining the effect of transmembrane peptides (Siegel et al., unpublished data) it became apparent that more detailed information on the kinetics of the L_α/Q_{II} phase transition in DOPE-Me was necessary. The situation is especially complicated by the delicate competition between transitions into the H_{II} and Q_{II} phases. Therefore, there were two primary aims for the current work. The first was to study the kinetics of lamellar/non-lamellar phase transitions in DOPE-Me, to determine if the observations were explicable in terms of a recently proposed theory of the transition mechanism (Siegel, 1999). The second was to determine the right conditions for use in a subsequent study of the effects of transmembrane peptides on non-lamellar phase formation in DOPE-Me (Siegel et al., in preparation).

Several types of time-resolved x-ray diffraction (TRXRD) experiments, including temperature jumps and temperature ramps in combination with differential scanning calorimetry (DSC), were used to obtain comprehensive data on the kinetics of the lamellar/non-lamellar phase transitions in DOPE-Me. The results are consistent with theoretical (Siegel, 1999) and experimental (Siegel & Epand, 1997) data on the phase transition mechanism, which suggest that H_{II} and Q_{II} phase formation from the L_α phase occurs through common intermediates.

In studies of the effects of peptides on the L_α/H_{II} and L_α/Q_{II} phase transitions, differences of a few degrees in transition temperature, or of hours in the time needed to form the Q_{II} phase, can be significant (Colotto et al., 1996; Colotto & Epand, 1997). We found that different lots of commercial DOPE-Me showed substantial differences in the values of the L_α/H_{II} transition temperature. There were also lot-to-lot differences in the time required for the Q_{II} phase to form in temperature-jump experiments. These results emphasize that studies of the effects of exogenous substances on non-lamellar phase formation in DOPE-Me should be performed with appropriate control for lot variability. In this and related work (Siegel et al., in preparation), we used a single lot of DOPE-Me for studies of the phase behavior and transition kinetics.

Materials and Methods

Buffers and Reagents

Both the free acid and sodium salt of N-tris[hydroxymethyl]methyl-2-aminoethanesulfonic acid (TES), and the disodium salt of ethylenediamine tetraacetate (EDTA), were obtained from Sigma (St. Louis, MO). NaCl was obtained from Fluka (Ronkonkoma, NY). Chloroform and methanol were both "Optima" grade from Fisher Scientific (Pittsburgh, PA). Solutions were made using water (resistivity >18 MΩ · cm) purified by a Milli-Q apparatus, with one charcoal, one Organosorb®, and two deionizing cartridges (Millipore, Bedford, MA). The standard buffer was 150 mM NaCl, 20 mM TES, 0.1 mM EDTA (pH 7.4 at room temperature (~22°C)).

DOPE-Me

DOPE-Me was obtained from Avanti Polar Lipids (Alabaster, AL) as a lyophilized powder, and was used without further purification. Samples were prepared using DOPE-Me from individual lot numbers 59–63, as supplied by the manufacturer. Lipid received from the manufacturer was >99% pure (*see* below), and was stored at −70°C until used for sample preparation.

In preliminary studies we noticed substantial lot variability in DOPE-Me transition temperatures (*see* Results section below). It was suggested that impurities in the N-monomethyl ethanolamine (MME) used in the synthesis of DOPE-Me might be responsible for such behavior. Accordingly, Lot 63 of DOPE-Me was synthesized using re-purified MME, as described below. All the data reported in this study was obtained using Lot 63 lipid, unless otherwise specified. MME was obtained from Aldrich (Milwaukee, WI) and purified by vacuum distillation. The first one-fourth of the MME was discarded during the initial distillation, and the next portion (approximately one-half of the original volume) was collected as a purified fraction. The distilled MME was stored in a sealed vessel at −20°C until used. MME was neutralized with concentrated hydrochloric acid by dropwise addition with stirring, using a pH meter. The MME was kept at temperatures below 15°C during neutralization, using an ice bath.

DOPE-Me was prepared by enzymatic treatment of 1,2-dioleoyl phosphatidylcholine (DOPC) with phospholipase D in the presence of neutralized MME, as described (Kates & Sastry, 1969). Reaction progress was monitored by thin layer chromatography (TLC) in chloroform:methanol:water (65:25:4 by volume). The TLC plates were visualized with ninhydrin spray to detect primary amines (Skipski, Peterson & Barclay, 1968) and molybdate spray to detect phosphorus-containing lipids (Ellington & Lands, 1968). Details on the preparation of these detection sprays can be found at http://www.avantilipids.com. The product was isolated and purified by normal phase silica gel column chromatography (40 μm particle size, 60 Å pore size) using chloroform/methanol-based solvents for elution, lyophilized, and stored at −70°C.

DOPE-Me produced using purified MME (Lot 63) was compared with DOPE-Me made with standard MME (Lot 62), using ^{1}H NMR and flow injection mass spectrometry. The ^{1}H NMR spectra were obtained with an ARX300 spectrometer (Bruker Instruments, Billerica, MA), using tetramethylsilane as an internal chemical shift resonance standard (0.00 ppm), with the DOPE-Me dissolved in deuterochloroform at 5 mg/mL. The ^{1}H NMR spectra revealed no differences between lots (*data not shown*). For the mass spectrometry, an Agilent Technologies (Alpharetta, GA) 59987A/5989A elecrospray-interface mass spectrometer (ESMS) was used. Samples of DOPE-Me were dissolved in chloroform:methanol:water (65:38:8 by vol.) with either 0.1% (v/v) 26% ammonium hydroxide for negative-mode ionization or 2% (v/v) glacial acetic acid for positive-mode ionization at a lipid concentration of 1 mg/mL. All solvents and chemicals were HPLC grade from Fisher Scientific (Fairlawn, NJ). The samples were manually injected (1 μL) into a 10 μL loop in-line with a continuous 20 μL/min flow stream of the appropriate solvent connected to the electrospray needle. The spray stream was directed off-axis to the capillary of the electrospray interface. The electrospray interface temperature was set at 150°C with the quadrupole temperature set to 110°C and 150°C for negative and positive ionization, respectively. The ESMS

was programmed to scan an m/z range of 200–1050 in positive mode and 200–1500 in negative mode. Mass resolution was optimized to 0.1 m/z. The capillary exit voltage was maintained at a low setting relative to the first skimmer lens to minimize fragmentation, and produced molecular ions of substantial abundances for interpretation. There was no apparent difference between the positive mode mass spectra for DOPE-Me from Lots 62 and 63. Both exhibited the $[M+H]^+$ ion at 758.5 ± 0.1 and $[M+Na]^+$ at 780.4 ± 0.1, as well as an unidentified ion at m/z = 603.5 at much lower intensity than the $[M+H]^+$ ion in each lot. In the negative mode mass spectra, the $[M\text{-}H]^-$ m/z of the DOPE-Me was 757.0 ± 0.1. Lot 62 exhibited an additional ion with m/z = 492.6 (corresponding to a monoacylated PE-Me where the acyl chain is a monoene, 18 carbon atoms long) and another unidentified ion at m/z = 829.0, while Lot 63 did not. However, both of these latter ions were present at very low intensity compared to the $[M\text{-}H]^-$ ion of DOPE-Me. The ESMS technique is not quantitative in the relative amounts of the different ionized species, because of order-of-magnitude differences in sensitivity of the technique to different ions. Neither the monoacylated PE-Me nor an impurity corresponding to the 829 m/z peak in the ESMS spectrum were detected in the NMR experiments on lipid from Lot 62. The sensitivity of the NMR method is such that impurities cannot be detected at levels < ca 1 mol%. The TLC data show that lipid in Lots 62 and 63 were both >99% pure, and the NMR and ESMS results did not detect major differences in composition between them. We conclude that the use of re-distilled MME in the synthesis of DOPE-Me has little effect on DOPE-Me purity.

Sample Preparation for X-ray Diffraction and DSC

DOPE-Me samples were made by two different protocols; direct hydration of lyophilized DOPE-Me powder, and lyophilization of lipid from a 1,1,1-trifluoroethanol (TFE)/water mixture (1:16 by vol.) before hydration. The latter was used to evaluate the effect, if any, the solvent mix had on DOPE-Me phase behavior. In a separate study, membrane-spanning peptides were to be introduced into DOPE-Me bilayers and the TFE -containing solvent was to be used for the initial co-solubilization (Siegel et al., in preparation). Thus the need for this control study. All DOPE-Me samples discussed in the present work were made with the TFE/water lyophilization method, unless stated otherwise.

Samples prepared by direct hydration were made by weighing lyophilized lipid (40–150 mg) into a 1 mL glass vial with a Teflon-faced cap (Wheaton, Millville, NJ), adding sufficient buffer to yield the desired final lipid weight concentration. An analytical balance (model R200D, Sartorius Company, Gottingen, Germany) with an accuracy of ±0.02 mg was used for this purpose. The lipid and buffer were quickly mixed mechanically with a stainless steel spatula and then by vortex mixing for 1 min (Vortex Genie 2, Fisher Scientific, Pittsburgh, PA) at room temperature, and the mixture was sealed under Argon and allowed to stand on ice for 1 h. During this time it was vortex-mixed for 1 min two additional times. The mixture was subjected to three freezing and thawing cycles, by immersing the vial for 5 min in powdered dry ice and for 2.5 min in water at room temperature, respectively. The mixture was vortex-mixed for 1 min following each thaw. Finally, the sample was transferred to DSC cells or to x-ray capillaries, as described below. The TFE/water samples were prepared as follows (Killian et al., 1996). Lyophilized lipid (35–70 mg) was hydrated in 0.25 mL Milli-Q water in a stoppered 15-mL Pyrex pear flask under Argon, quickly vortex-mixed for 1 min at room temperature, and allowed to equilibrate for 1 h on ice. The suspension was vortex-mixed for an additional minute prior to further treatment. At this point in the peptide/lipid incorporation procedure (Killian et al., 1996), peptide would be added as 0.25 mL of a solution in TFE. To mimic this step, 0.25 mL of pure TFE was added to the DOPE-Me/water dispersion, and the mixture was vortex-mixed for 1 min at room temperature. The TFE/water lipid suspension was much less turbid and viscous than the original lipid suspension in water. The suspension was diluted with 3.75 mL ice-cold Milli-Q water, added in three equal portions with a few seconds of vortex mixing after each addition, followed by 1 min of vortex mixing after the final portion was added. The suspension was shell-frozen by swirling the flask in a liquid nitrogen bath. It was lyophilized overnight at room temperature. The vacuum system was home-built and included two liquid nitrogen traps. The final pressure in the vacuum system at the end of the lyophilization procedure was < 20 milliTorr. The lyophilized powder was weighed into a plastic 1.5 mL Eppendorf centrifuge tube, hydrated to 33% (w/w) DOPE-Me with TES buffer, vortex-mixed for 1.5 min at room temperature, and allowed to equilibrate on ice for 1 h. It was again vortex-mixed, and subjected to six freeze/thaw cycles (dry ice/room temperature water) with 30 s of vortex-mixing after each thaw.

DSC

DSC was performed on samples of DOPE-Me made by the direct hydration method, using a CSC 4100 calorimeter (Calorimetry Sciences, Provo, UT). Samples were transferred from vials into the tared DSC cells by Pasteur pipet and spatula, and the cells were re-weighed to obtain the exact amount of lipid in each. The reference cell was filled with a weight of Milli-Q water that was within 5% of the weight of the mixture in the sample cells. Thermograms were obtained at the specified temperature scan rates. (The temperature scan rate is almost, but not absolutely, uniform across the entire range, so the exact rates across the transition temperature interval were determined after the experiments by reading the time necessary to scan between 60 and 66°C from the data files.) For temperature scan rates slower than 4°C/h, the samples were incubated at 55°C for 90 min before the scan was started from that temperature. This protocol was used because previous experience (Siegel & Banschbach, 1990) showed that it speeds nucleation of Q_{II} phases at higher temperatures, and the Q_{II} phases are only observable at the slowest temperature scan rates. Computer software supplied with the calorimeter was used to correct the thermograms for the time constant of the instrument, to subtract a baseline from peaks, and to evaluate the enthalpy change per mole of DOPE-Me for the observed phase transitions. The lipid concentrations in the DSC samples were between 15 and 33% (w/w) of DOPE-Me. The calibration of the DSC was checked with samples of hydrated dipalmitoylphosphatidylcholine (DPPC), which yielded a P_β/L_α phase transition temperature of 41.25°C at a scan rate of 10°C. This value is almost exactly the average of the values (41.3 ± 1.8°C) deposited in LIPIDAT (http://www.lipidat.ohio-state.edu; Koynova & Caffrey, 1998). Enthalpy values were calibrated using ice melting at 0°C.

Introduction of DOPE-Me into X-ray Capillaries

Small amounts of hydrated DOPE-Me (ca. 10 mg) were placed in the funnel end of 1.0 mm diameter quartz x-ray capillaries (Charles Supper Co., Natick, MA) with a stainless steel spatula. The capillaries were then placed in plastic 15 mL conical-bottom centrifuge tubes and centrifuged in a swinging-bucket rotor at low speed until the mixture was forced to the bottom of the capillary (1,070 × *g*, 2 min; Clinical centrifuge, IEC International Equipment, Needham Heights, MA). An additional 1.5 μL of buffer was added to each

capillary and centrifuged in the same fashion to wash down the walls, which made the final lipid concentration approximately 30% (w/w). The capillary was then flame-sealed with a microtorch (Microflame, Minnetonka, MN). Small beads of 5 min epoxy cement were placed on the sealed ends to protect the fused joints. To ensure homogeneity of the lipid/buffer samples in the capillaries, they were mixed by pelleting the sample mixture from one end of the capillary to the other. This was done by inverting the sealed capillaries, placing them in water-filled 1.5 mL Eppendorf tubes at room temperature, and centrifuging the tubes at 14,000 rpm in an Eppendorf microcentrifuge (model 5415, Brinkman Instruments, Westbury, NY). The tubes were then removed, inverted again, replaced in the Eppendorf tubes, and the centrifugation process repeated until the lipid/buffer mixture had been cycled back and forth three times between the ends of the capillaries. Capillaries were stored at −70°C until they were used (within 27 d). Samples stored for 10 and 27 d under these conditions yielded the same Q_{II} phase development kinetics at 59.7°C (*data not shown*).

Rotating-Anode X-ray Diffraction

Static and time-resolved measurements were performed using a rotating-anode x-ray generator (Rigaku RU-300) producing Ni-filtered Cu K_α radiation (wavelength, $\lambda = 1.5418$ Å). Samples in quartz capillaries were placed in a specially designed sample holder (Zhu & Caffrey, 1993). The temperature inside the sample holder was controlled by two thermoelectric Peltier-effect elements regulated by a computer feedback system. Thermocouple measurements within capillaries in the capillary slots confirmed that the system could make fast temperature jumps at rates of 20°C/min to temperatures accurate to within 0.2°C, and to continuously increase the temperature at pre-programmed rates, in the temperature range from room temperature to 90°C. The thermocouple thermometer used for calibration of the temperature in the sample holder was a BAT-12 unit with an IT-23 probe (Physitemp Instruments, Clifton, NJ). The accuracy of the thermocouple thermometer was checked in 5 L of rapidly-stirred water against a mercury thermometer that was certified as accurate to within 0.02°C in the range 0–55°C using NBS-traceable standards (model ASTM 64C-FC, Ever Ready Thermometer, West Patterson, NJ). At 25°C, 36°C, and 52°C, the readings of the thermocouple and mercury thermometers agreed to within 0.2°C or less. Temperature inside the sample holder was regulated using feedback from a thermistor positioned close to the samples with a stability of 0.01°C. The sample holder could be moved in both the vertical and horizontal directions by stepper motors. The samples were usually moved continuously back and forth along the capillary axis (total travel = 3 mm, speed = 3 mm/min) to average the contributions to total scattering from different parts of the sample and to minimize possible radiation-damage effects during long exposures. The x-ray beam was focused by two curved Ni-coated mirrors (Charles Supper, Natick, MA) to a spot size of ca. 0.5 mm × 0.5 mm at the detector position. The sample-to-detector distance (in air) was measured using silver behenate standards (58.4 Å; Blanton et al., 1995), and was usually 340 mm. High-resolution image plates, 200 mm × 250 mm (HR-IIIn, Fuji Medical Systems, Stamford, CT) were used to record diffraction patterns. X-Ray images from the image plates were scanned after exposure, using a phosphor image scanner (Storm-840, Molecular Dynamics, Sunnyvale, CA) with a resolution of 100 μm. We used a home-built streak camera (Zhu & Caffrey, 1993) to monitor changes in the diffraction pattern from a sample continuously with increasing time or temperature. It consisted of a narrow vertical slit (width of 2–3 mm) and a stepper motor mechanism for continuously moving the image plate past the slit. The experimental conditions (temperature, sample and detector movements) were controlled by a computer program written in the LabView language (National Instruments). Intensity versus scattering vector q ($q = 4\pi\mathrm{Sin}(\vartheta)/\lambda$, where 2ϑ is the scattering angle) plots were obtained by radial integration of static two-dimensional powder diffraction patterns using the FIT2D program (Hammersley et al., 1996; Hammersley, 1997). The I–q scattering profiles were fitted with the Peakfit 4.0 program (SPSS, Chicago, IL). For all measurements, DOPE-Me samples were removed from the −70°C freezer, allowed to warm up to room temperature for a few minutes, loaded into the x-ray sample holder, and were then incubated for 1 h at 55°C before either a temperature jump to the desired observation temperature or a temperature ramp during TRXRD measurements.

Synchrotron Source X-ray Diffraction

Time-resolved small-angle x-ray diffraction measurements were performed on the X-12B beamline at NSLS (Brookhaven National Laboratory, Upton, NY). A monochromatic x-ray beam (energy, $E = 8.979$ keV; $\lambda = 1.38$ Å) was focused at the detector position with a sample-to-detector distance of 125.5 cm, determined using silver behenate. Diffraction patterns were recorded with a 2-D gas wire detector (10 cm × 10 cm, 508 × 496 pixels; Capel, Smith & Yu, 1995). The same temperature-controlled sample holder used in the rotating-anode experiments was used in the synchrotron experiments, but the sample was stationary in the synchrotron experiments to maintain better alignment. In the temperature ramp and temperature jump experiments, data were collected in 1-min exposures at intervals of several minutes. The shutter was closed between exposures to minimize radiation damage. For the temperature scan between 55.6 and 61.9°C, an initial 1-min exposure was followed by thirty 1-min exposures at 8-min intervals, which corresponds to a temperature interval between exposures of 0.2°C. For the temperature jump from 55 to 61.7°C, an initial 1-min exposure was followed by thirty 1-min exposures at 5-min intervals. For the temperature jump from 55 to 67.1°C, twenty consecutive 1-min exposures were followed by eight 1-min exposures at 5-min intervals and three 1-min exposures at 10-min intervals. Raw data were compensated for detector response using an exposure obtained without a cell in the beam and with the sample-to-detector path filled with air. The data were radially integrated using beamline software (description posted at http://x12wulfgar01.nsls.gov/x12b_info.html). The radially-integrated diffraction patterns were fitted with the Peakfit 4.0 program. The relative diffracted intensities produced by different phases were determined as follows. In radially-integrated diffraction patterns, the individual peaks were fitted to Gaussian functions after baseline subtraction. The intensities of selected diffraction peaks associated with each phase were then summed. The Miller index of peaks chosen in each case follows: lamellar phase, (001), (002); Q_{II}-Pn3m, (110), (111); Q_{II}-Im3m, (110), (200), (211); H_{II}, (10), (11), (20). These reflections were chosen because they clearly identified the given phase, they were usually reasonably well resolved, and they represented most of the diffracted intensity in a given pattern.

Radiation Damage

Radiation damage from strong synchrotron sources can easily compromise results of a diffraction experiment. A typical manifestation of radiation damage in lipid systems is a lowering of the apparent lamellar/non-lamellar phase transition temperature (Cheng & Caffrey, 1996; Cherezov, Riedl & Caffrey, 2002). To look for damage, we exposed a stationary capillary containing hydrated DOPE-Me continuously for 1 h to 8.979 keV x-rays at beam line X-12B. The exposure was done at 57°C, which is 2°C below the temperature at which Q_{II} phases first form in this system, as

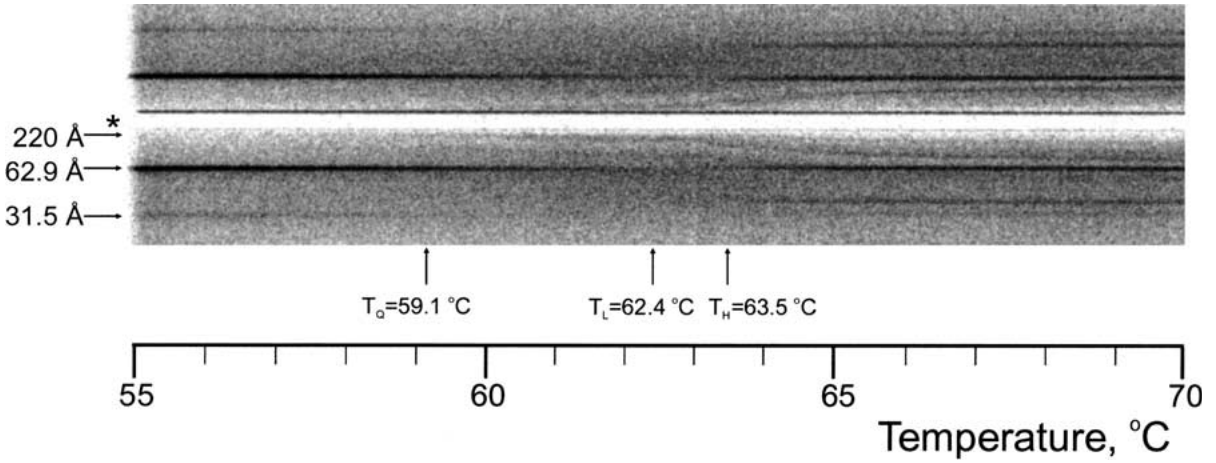

Fig. 1. Rotating-anode streak camera diffraction pattern obtained from a sample of hydrated DOPE-Me during a heating scan from 55 to 70°C. The temperature scan rate was 1.5°C/h. The sample-to-detector distance was 340 mm. The image plate was moved behind a 3 mm slit at a speed of 0.3 mm/min. The asterisk (*) identifies the position of the beam stop. Repeat distances and the temperatures at which the different phases come and go are identified and are explained more fully in the text.

determined by a synchrotron-based temperature-ramp study at 1.5°C/h on duplicate samples. Data, collected in the form of sixty successive 1-min exposure diffraction patterns, revealed the presence of lamellar phase only for the duration of the experiment. This is taken as evidence that the sample did not succumb to radiation damage. Further, immediately after the 60min exposure, diffraction patterns were obtained from adjacent, unexposed regions of the same sample. They were nearly identical to those obtained from the spot exposed continuously for 60 min. To put this in context, typical exposures of DOPE-Me specimens in the current study are of 40 min duration or less. Our conclusion therefore is that x-ray damage is not an issue in this study.

Thin-layer Chromatography

Thin layer chromatography (TLC) was used to determine the extent to which DOPE-Me degraded at the high temperatures used in this study. Accordingly, lipid samples in capillaries were incubated for various times at 58 and 62°C. The capillaries were then placed in 1.0 mL conical-bottom glass vials (Wheaton, Millville, NJ), and crushed with a a glass rod. Chloroform was added at an approximate volume/lipid weight ratio of 10:1. The vial was sealed with a Teflon-faced cap, wrapped with Teflon tape, vortex-mixed, and stored at −20°C for between 1 and 24 h. For each sample, a 1 μL aliquot of the chloroform layer in the vial was applied to a TLC plate. In each case, a 1 μL aliquot of a 1:100 (v/v) dilution of the chloroform layer with chloroform was applied as a separate spot, to serve as an intensity reference on the developed plate. The TLC plates (Adsorbosil Plus Prekote plates, Alltech Associates, Deerfield, IL) were pre-washed twice with chloroform/methanol (2:1 (v/v)). The developing solvent was chloroform/methanol/water 80:20:2 (by vol). Plates were developed by spraying with 4.2 M sulfuric acid and charring on a hot plate (200°C). The extent of degradation was estimated visually by comparing the intensity of minor spots on the plates with the intensity of the 1:100 dilution spots. In samples incubated for 7 h at 58 and 62°C, contaminant spots were visible that represented substantially less than 0.5% of the total intensity. In samples incubated for 20 h at 58 and 62°C, the combined intensity of these spots was approximately 0.5% that of the main spot. In comparison, Siegel & Banschbach (1990) found that degradation of 1 mol% DOPE-Me sample (modeled by addition of 1 mol% lyso-phosphatidylethanolamine and 1 mol% oleic acid) produced only a 1°C change in transition temperature in DSC experiments at scan rates of 9°C/h. Thus, it is unlikely that degradation products produced during up to 10 h of incubation at 62°C had a significant effect on DOPE-Me phase behavior in the current study.

Results

X-ray Diffraction

TRXRD was used to determine the identities of non-lamellar phases that formed in DOPE-Me, the temperatures at which they formed in temperature-ramp experiments, and the times required for their formation in samples subjected to temperature jumps. Three types of TRXRD experiments were performed. The first was a rotating anode-source streak camera experiment, in which a one-dimensional diffraction pattern was obtained from a sample exposed continuously as a function of time, either after a temperature jump or during a temperature ramp. We used this technique primarily to identify the temperatures at which Q_{II} and H_{II} phases emerged from the L_α phase in samples of DOPE-Me. Figure 1 shows data obtained while DOPE-Me was heated continuously at 1.5°C/h from 55°C, where the L_α phase prevails, to 70°C. A very low-angle reflection arising from a Q_{II} phase appears at 59.1°C. This solitary and faint reflection has a d-spacing of approximately 220 Å, and is located close to the beam stop (asterisk) in Fig. 1. A single reflection is insufficient to index a phase, but it does serve to show that a new phase began to form at this temperature. Separate synchrotron and rotating-anode measurements confirm that this reflection is from a cubic phase (*see* below). At 62.4°C, the diffraction lines from the L_α phase

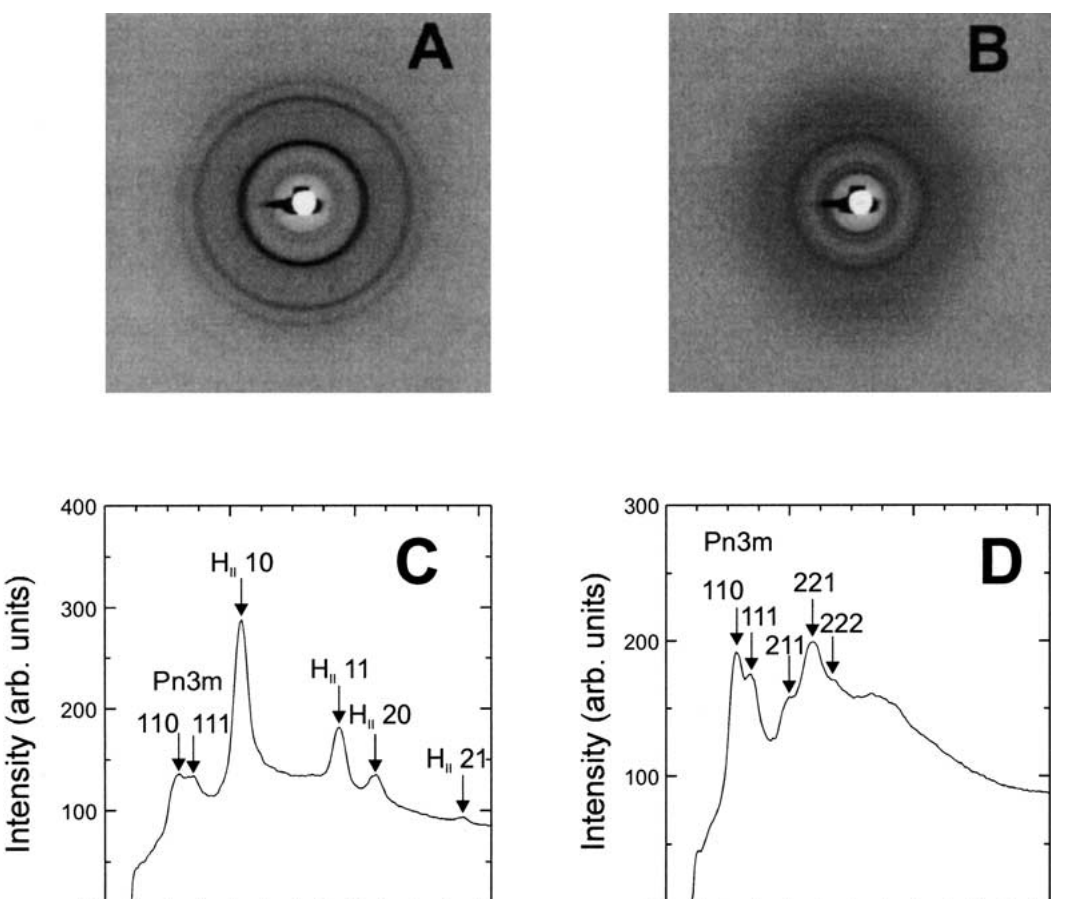

Fig. 2. Diffraction patterns obtained from hydrated DOPE-Me after a temperature jump from 55 to 64.6°C recorded using a rotating-anode x-ray source. *A* and *B* are two-dimensional diffraction patterns recorded between 0 and 120 min and between 180 and 300 min after the temperature jump, respectively. Radially-integrated intensity versus scattering vector plots of the patterns in *A* and *B* are shown in *C* and *D*, respectively. Miller indices for the different phases are indicated.

disappeared, and at 63.5°C reflections from the H_{II} phase became visible. These streak-camera experiments were not sensitive enough to reliably identify the type of Q_{II} phase present (Q_{II}-Im3m, Q_{II}Pn3m, etc.) or to provide accurate values of the Q_{II} phase lattice constants.

In the second type of TRXRD experiment, two-dimensional x-ray diffraction patterns were collected, again using a rotating anode source. Examples are shown in Fig. 2*A* and *B*, which are successive diffraction patterns obtained on a sample pre-incubated for 1 h at 55°C and then jumped in temperature to 65°C. The patterns were recorded in the interval 0 to 120 min (Fig. 2*A*) and 180 to 300 min (Fig. 2*B*) after the jump. They show the presence of coexisting Q_{II} and H_{II} phases after 120 min (Fig. 2*A* and *C*), and only the Q_{II} phase after 300 min (Fig. 2*B* and *D*). The Q_{II} phase is of the Pn3m type with a lattice constant of 177 ± 2 Å, as defined by five reflections. While this second form of data collection provides more detailed diffraction patterns that, in turn, facilitate phase identification and microstructure characterization, it does not have the time resolution afforded by the streak-camera method. Accordingly, we resorted to streak-camera experiments for time-resolved studies and for an overview of phase behavior, and to successive two-dimensional diffraction pattern measurements to confirm the phase assignments and to measure lattice parameters.

The third type of TRXRD experiment was synchrotron-based where successive two-dimensional diffraction patterns were obtained during a temperature ramp, or following a temperature jump. Thus, for example, Fig. 3 shows selected results of one such ramp experiment in which the sample was heated continuously from 56.0 to 61.8°C at 1.5°C/h. Diffraction patterns were obtained with 1-min exposures corresponding to intervals of 0.2°C. Figure 3*A*

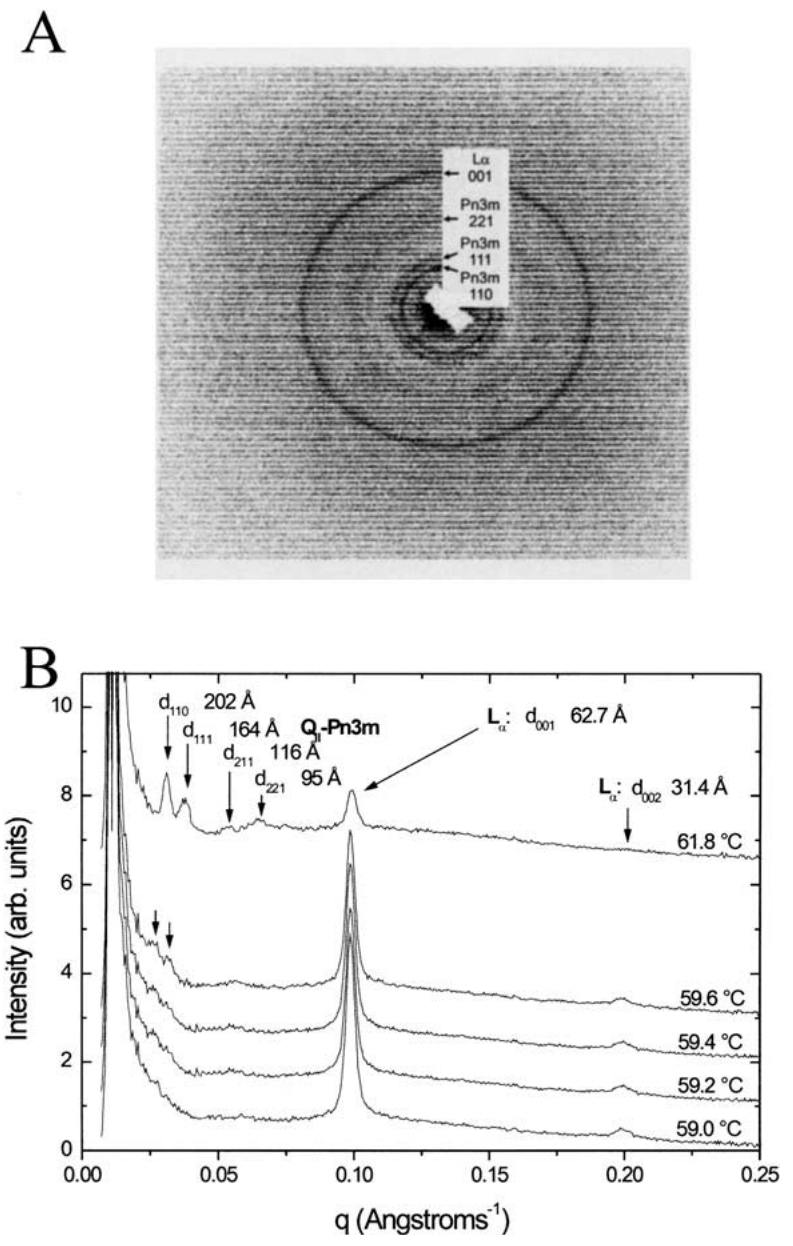

Fig. 3. Diffraction from hydrated DOPE-Me recorded during a temperature ramp from 56 to 61.8°C at a rate of 1.5°C/h using a synchrotron source. (*A*) Non-corrected two-dimensional detector image. The pattern was the last in a series obtained during the scan. Exposure time is 1 min at 61.8°C. (*B*) Radially-integrated diffraction patterns recorded during the scan. The patterns were collected at temperature intervals of 0.2°C. Temperatures, phases and their Miller indices are indicated.

shows the last two-dimensional pattern obtained in this series, at a temperature of 61.8°C. Radially-integrated patterns from the same series are shown in Fig. 3*B*. The only peaks in the pattern at 59.0°C are the (001) and (002) reflections from the L_α phase, at q = 0.1 and 0.2 $Å^{-1}$, respectively. At slightly higher temperatures, additional peaks appear at q = 0.026 and 0.032 $Å^{-1}$: these are clearly discernible at 59.6°C (*arrows*), along with a higher-q peak, which is probably a number of superimposed reflections from the Q_{II} lattice. These two peaks are at q values in the correct ratio to correspond to the (110) and (111) reflections from a Q_{II}-Pn3m lattice. In the last frame at 61.8°C (Fig. 3*A*), the four reflections with indices (110), (111), (211), and (221) from a Q_{II}-Pn3m lattice (*arrows*) are clearly visible. While this series appears to be missing the (200) and (220) reflections, they are known to be weak in the Q_{II}-Pn3m phase of DOPE-Me (Gruner et al., 1988; Siegel & Banschbach, 1990). Further, the (220) and (221) reflections are not well resolved but could be identified by peak-fitting procedures. Taken together, these data suggest that the Q_{II} phase formed under current circumstances is of the Pn3m type, and that it first appeared from within the bulk L_α phase at 59.6°C. Of the three TRXRD measurements just described, those done at the synchrotron are far superior in terms of diffraction quality and speed of data collection. However, since beam time is so limited, only selected studies could be done with this powerful x-ray source.

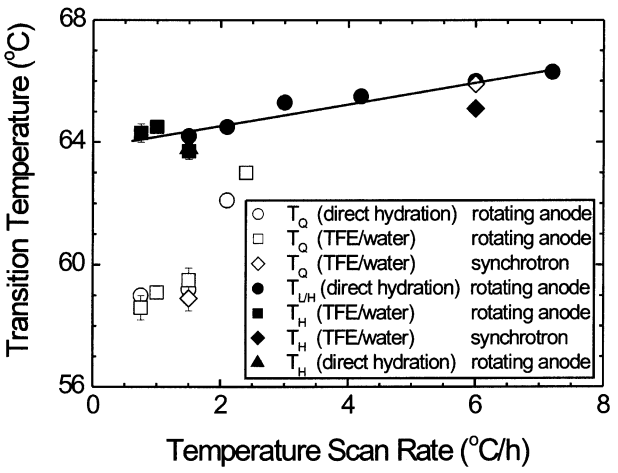

Fig. 4. Heating scan-rate dependence of the phase transition temperatures in hydrated DOPE-Me observed by x-ray diffraction in the 58 to 68°C range. The error bars indicate the standard deviation of transition temperatures recorded in multiple scans. Data points without error bars are results of single experiments. The transition types and the instruments used for the diffraction measurements are shown in the inset.

Ramp Rate-dependence of Transition Temperatures

The temperature ramp rate-dependence of non-lamellar phase appearance in DOPE-Me is shown in Fig. 4. The TRXRD experiments were performed with both rotating anode and synchrotron sources at scan rates ranging from 0.75°C/h to 7.2°C/h. We report on three characteristic temperatures: the temperature of the lamellar/inverted hexagonal phase transition, $T_{L/H}$, determined as the midpoint of the transition; the temperature at which the H_{II} phase first appears, T_H, for cases where loss of the lamellar phase precedes H_{II} phase emergence; and the temperature at which the Q_{II} phase first appears, T_Q. To assist the reader in tracking these assorted transformations, a schematic of the time- and temperature dependent changes in phase behavior observed in temperature ramp and jump experiments is presented in Fig. 5. Here, the three transition temperatures just mentioned are defined operationally.

One of the first conclusions to emerge from the data in Fig. 4 is that sample preparation mode has no effect on phase behavior. Thus, samples prepared by direct hydration or by lyophilization from TFE yield very nearly the same phase transition temperatures at the same ramp rates. This is an important result, use of which will be made in a subsequent study as outlined in the Introduction.

Temperature-ramp experiments show that there are three distinct phase-behavior types operating under different scan-rate conditions (Figs. 4 and 5*A*). Thus, at slow scan rates of <2°C/h (Fig. 5*A*1), a direct L_α/Q_{II} transition takes place first with T_Q ranging from 58 to 60°C depending on actual rate. As temperature increases, the Q_{II} phase emerges and grows at the expense of the L_α phase. With time and temperature, the H_{II} phase appears ($T_H = 64$°C), which then coexists with the Q_{II} phase for the duration of the experiment. This type of scan was implemented in a later study designed to examine the effects of membrane-spanning peptides on T_Q (Siegel et al., in preparation).

At intermediate scan rates of 2–3°C/h, the Q_{II} phase appears at a slightly higher temperature ($T_Q \sim$ 62-63°C) than was observed at the lower rates (Fig. 5*A*2). It coexists with the lamellar phase for a spell, and at 64°C the L_α/H_{II} transition occurs. Thereafter, the Q_{II} and H_{II} phases coexist up to 70°C.

At the highest scan rates (>3°C/h) examined, the L_α/H_{II} transition precedes any significant accumulation of Q_{II} phase (Fig. 5*A*3). Thus, the cubic phase is either not observed up to 70°C (rotating anode, 3–6°C/h) or it forms at about the same temperature that the H_{II} phase appears (synchrotron, 6°C/h). In the latter synchrotron experiment, $T_{L/H}$ was 64.7°C, while T_Q was 65.9°C. The appearance of the Q_{II} phase in the synchrotron but not in the rotating-anode data, may be attributed to the greater sensitivity of the former. It is also possible that the L_α/Q_{II} transition simply does not occur at a reproducible temperature at these relatively fast scan rates.

Identity and Lattice Constant of the Q_{II} Phase Formed in Temperature-Ramp Experiments

The Q_{II} phase that first formed in all temperature-ramp experiments was of the Q_{II}-Pn3m type (Figs. 2 and 3). This was also the phase identified in 33% (w/w) DOPE-Me at temperatures between 61 and 62°C by Siegel and Banschbach (1990). Figure 6*A* shows the relative diffracted intensities of the different phases as a function of temperature for the ramp experiment in Fig. 3. The intensity of the lamellar phase decreases continuously with increasing temperature. The Q_{II}-Pn3m phase appears at 59.6°C and its diffracted intensity increases continuously thereafter.

In a separate study, a decrease in the lamellar phase diffracted intensity was observed during incubations at a fixed temperature just below T_Q (55°C for example; *data not shown*). This is consistent with a gradual disordering of the L_α phase accompanied by the formation of Q_{II} phase precursors below T_Q (Gagné et al., 1985; Ellens et al., 1989; Siegel et al., 1989b; Siegel et al., 1994).

In Fig. 6*B*, the lattice constants of the lamellar and Q_{II} phases are displayed as a function of temperature. The lattice parameter of the lamellar phase is relatively insensitive to temperature, changing by less than 0.5 Å in the range studied. In contrast, the

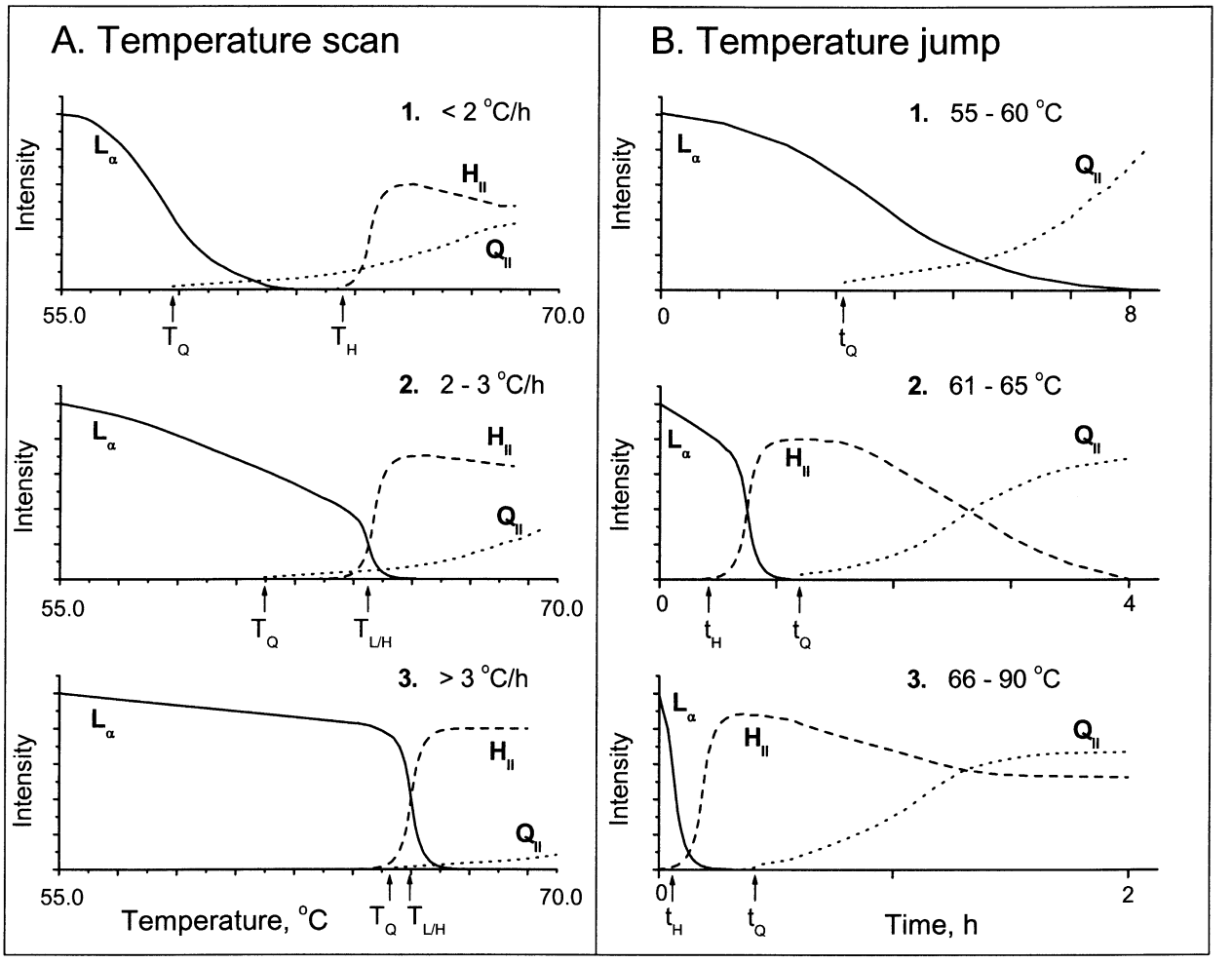

Fig. 5. Schematic representation of phase evolution during temperature ramp (*A*) and temperature jump (*B*) measurements made with hydrated DOPE-Me. In the ramp studies, the phase evolution profile depends on scan rate, as indicated. In the temperature jump studies, the phase evolution profile depends on final temperature, as indicated. The identities of the phases are shown along with the temperatures (*A*) and times (*B*) of critical events in the evolving phase profile. These schematics are based on ramp data in Fig. 4 and on jump data in Fig. 7.

lattice constant of the Q_{II}-Pn3m phase falls steadily and quite dramatically with temperature. While phase-type identification was done with some trepidation at low temperature (59.6°C) based as it was on just two reflections, at higher temperatures five reflections were clearly visible and were used with confidence in indexing the phase.

Kinetics of Q_{II} and H_{II} Phase Appearance in Temperature-Jump Experiments

The data above indicate that the sequence of phases observed when DOPE-Me is heated depends on temperature-ramp rate. It seems reasonable to propose therefore that the relative rates of the L_α/Q_{II} and the L_α/H_{II} transitions are temperature-dependent. This dependence was examined in more detail by following the system's response to temperature jumps. To this end, sample temperature was rapidly (within ca 30 s) changed from a value below T_Q (55°C) to a higher value, after which x-ray diffraction patterns were recorded as a function of time at the constant final temperature. The results are shown in Fig. 7. A simplified schematic representation of the data is presented in Fig. 5*B*. As the final temperature to which the sample was rapidly adjusted (jumped) increased, the time taken for Q_{II} phase to form dropped almost exponentially (Fig. 7*A*). Thus, the Q_{II} phase formed in 9 min following a temperature jump to 67°C. In contrast, when the jump was to 55°C, the Q_{II} phase formed after 5 to 7 h. Given the sluggish nature of the transition at low temperatures, it would be difficult to determine the true T_Q, since whether or not Q_{II} phase forms at a given low temperature depends on how long one is willing to wait. Parenthetically, we note that no Q_{II} phase was observed at 52.8°C after an incubation period of 9 h. Further, we chose not to perform experiments with

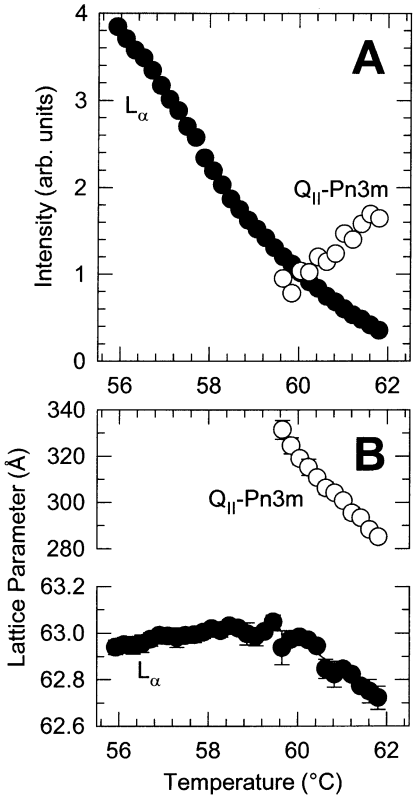

Fig. 6. Temperature-dependence of the relative diffracted intensities (*A*) and lattice constants (*B*) of the phases detected in the temperature ramp experiment shown in Fig. 3. The scan rate was 1.5°C/h. The diffracted intensities were calculated as described in the Materials and Methods section. The intensity associated with the Q_{II} phase has been multiplied by a factor of four to facilitate comparison with the greater intensity from the lamellar phase.

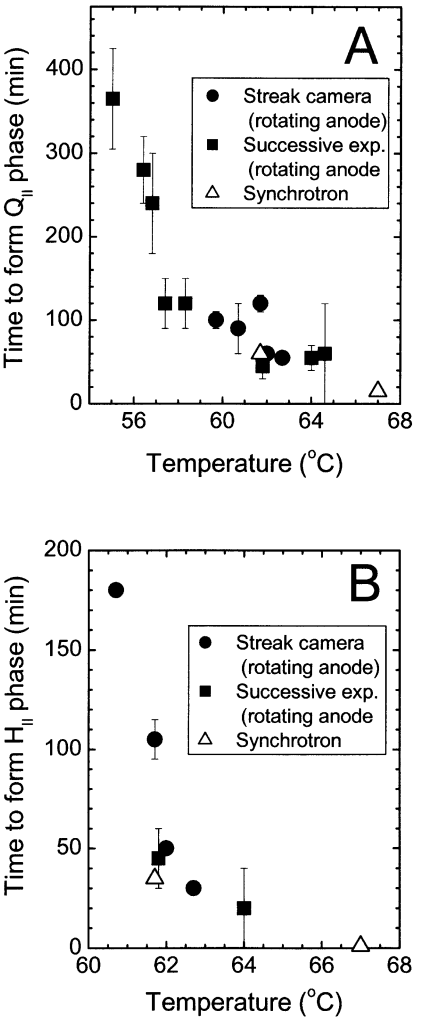

Fig. 7. Time to form either the Q_{II} phase (*A*) or the H_{II} phase (*B*) from the L_α phase of hydrated DOPE-Me following rapid temperature jumps from 55°C to the indicated final temperatures. The error bars represent the range of times deduced from multiple streak-camera experiments or uncertainties due to the finite exposure time for successive exposures (time between the end of one exposure and the end of the following exposure). The x-ray source used and the type of data collection mode are indicated in the key.

incubation times longer than 12 h because of possible artifacts associated with chemical degradation at these relatively high temperatures (*see* Materials and Methods).

As with Q_{II}, the H_{II} phase also formed with delay times that rose rapidly with decreasing temperature (Fig. 7*B*). Moreover, although there is a lot of variation in the time lag for Q_{II} and H_{II} phase formation between duplicate experiments, the H_{II} phase consistently formed before the Q_{II} phase in all seven experiments performed at and above 61°C. In contrast, at 60.7°C, one replicate of a duplicate yielded the Q_{II} phase after 120 min but no H_{II} phase formed up to 600 min. The other replicate produced the Q_{II} phase at 60 min and the H_{II} phase at 180 min. At and below 59.7°C, the H_{II} phase did not appear in measurements performed with observation times of 8–10 h. We conclude therefore that the H_{II} phase can begin forming in DOPE-Me after jumps to temperatures in excess of 60°C. Above this limiting temperature, the H_{II} phase formation precedes that of the Q_{II} phase. The delay between H_{II} and Q_{II} phase formation varies with temperature. Figure 7 shows that the delay is 20–40 min at 61.7°C and that it drops to 9 min at 67°C. However, the delay increased at very high temperatures. For example, in rotating-anode temperature jumps to 80.6°C and to 90.3°C, H_{II} phase formed immediately (<15 min), but the Q_{II} phase formed only after incubations of 1–2 h (*data not shown*). The results of these temperature jumps are summarized in Fig. 5*B* where three behavior types are apparent. Jumps to 55–60°C are characterized by a gradual disappearance of the L_α phase and an equally gradual growth of the Q_{II} phase (Fig. 5*B1*). No H_{II} phase forms at these low temperatures. Jumps to 61–65°C give rise to a direct L_α/H_{II} transition subsequent to which is the emergence of the Q_{II} phase (Fig. 5*B2*). The latter coexists with the H_{II} phase and,

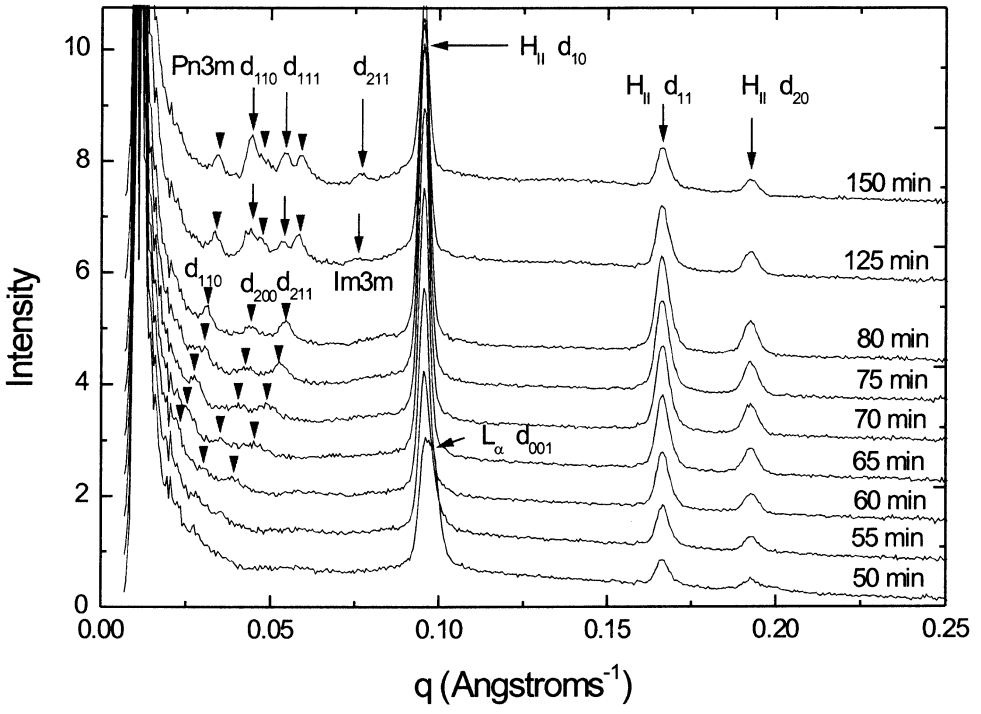

Fig. 8. Radially-integrated diffraction patterns obtained from hydrated DOPE-Me, which was jumped from 55 to 61.7°C in a synchrotron experiment. Diffraction patterns were obtained at 5-min intervals after the temperature jump. Elapsed times, phases and their Miller indices are indicated.

with time, replaces it completely. At the end of such a temperature-jump experiment, only Q_{II} phase remains. At jumps to the highest temperatures used in this study (66–90°C), there is again a rapid and direct L_α/H_{II} transition (Fig. 5*B3*). This is followed by growth of the Q_{II} phase and a prolonged period (out to 12 h) of Q_{II}/H_{II} phase coexistence. These data suggest that the H_{II} phase that forms in the 66–90°C range is stable. In contrast, it is metastable with respect to the Q_{II} phase in the range from 61 to 65°C.

Synchrotron data have been collected on this system following a temperature jump and the results are presented in Fig. 8. The data provide evidence for the formation of two cubic phases (with space groups Pn3m and Im3m) in the post jump period. The experiment was done by first pre-incubating the sample for 1 h at 55°C and then jumping it to 61.7°C, after which diffraction patterns were collected at 5 min intervals. 35 min following the jump, the diffraction pattern shows that the L_α and H_{II} phases coexist. Unfortunately, the (001) reflection of the lamellar phase and the (10) reflection of the H_{II} phase overlap, as shown in Fig. 8. However, the (11) reflection at $q = 0.17$ Å^{-1} from the latter is clearly resolved and can be used to track this phase in isolation. In the interval between 50 and 75 min, the H_{II} phase grows at the expense of the L_α phase. At about 60 min, the Q_{II}-Im3m phase makes its appearance as a series of three, very low-angle reflections. With time, these move together to higher angles, corresponding to smaller unit cell sizes. Eventually, tell-tale reflections from the Q_{II}-Pn3m phase appear, which persist along with those of the Q_{II}-Im3m phase for the duration of the experiment. The relative intensities of the diffraction from these assorted phases, as well as phase microstructure, during the course of this experiment are presented in Fig. 9*A*.

Figure 9*B* is a plot of the Q_{II}-Im3m and Q_{II}-Pn3m phase lattice constants as a function of time after the temperature jump. The lattice constant of the Q_{II}-Im3m phase is 347Å when it first forms, and decreases rapidly (by about 20%) over the next 15 min. The initial Q_{II}-Pn3m phase lattice constant is 209 Å, and it, too, falls with time. The inset to Fig. 9*B* is a plot of the ratio of the lattice constants of the Q_{II}-Im3m and Q_{II}-Pn3m lattices as a function of time throughout the temperature-jump experiment. These two appear to be in a nearly constant ratio of 1.30, which is close to the expected value of 1.28 (Hyde et al., 1984). This lends credence to the Q_{II}-Im3m phase assignment to the first cubic lattice that forms in the post-jump period, despite the fact that only three reflections were available for indexing. Separate rotating-anode measurements, where samples were monitored for longer times after the temperature jump, showed that only Q_{II}-Pn3m phase was present after several hours of incubation (*data not shown*).

In another synchrotron-based experiment, the sample was jumped to 67.0°C, in which case the two cubic phases formed simultaneously. Shortly

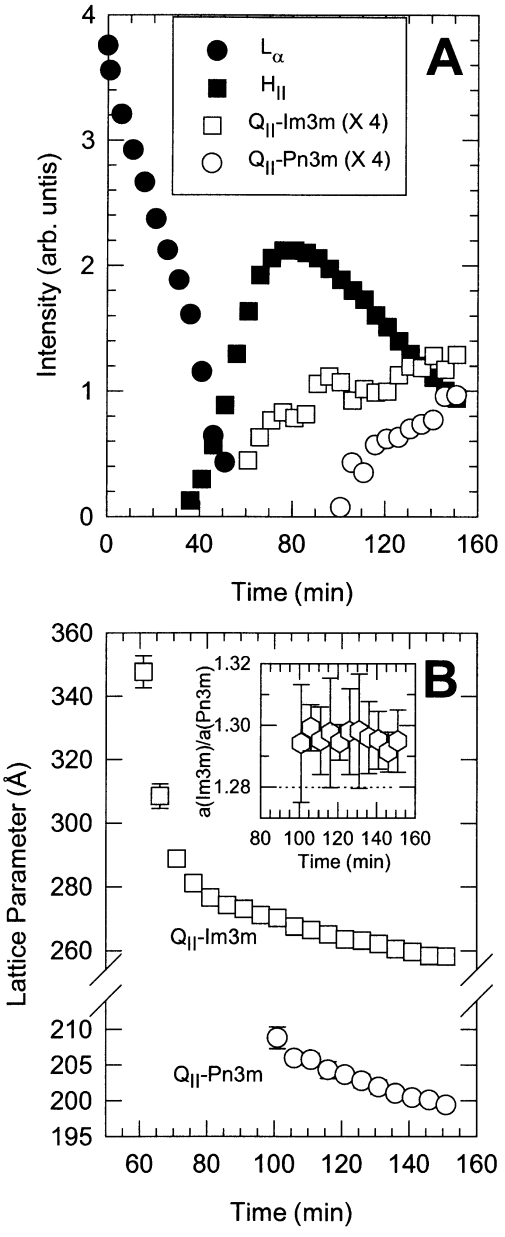

Fig. 9. Relative diffracted intensities (*A*) and lattice constants (*B*) of the phases present in hydrated DOPE-Me following a temperature jump from 55 to 61.7°C. These data are for the same experiment as reported in Fig. 7. *Inset*: dependence of the ratio of the lattice parameters of the Q_{II}-Im3m and Q_{II}-Pn3m phases on time.

thereafter, the Q_{II}-Im3m phase faded and only the Q_{II}-Pn3m phase remained after 90 min (*data not shown*).

Equilibrium Values of the Q_{II}-Pn3m Lattice Parameter as a Function of Temperature

Figure 10 is a plot of the lattice parameter of the Q_{II}-Pn3m phase as a function of temperature, determined using the rotating-anode x-ray source. The data were

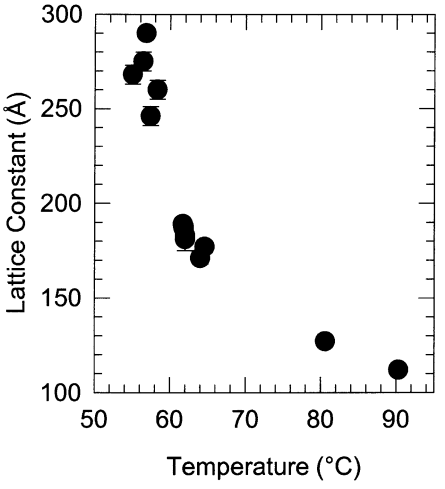

Fig. 10. Temperature dependence of the lattice constant of the Q_{II}-Pn3m phase in hydrated DOPE-Me. Data were obtained on samples incubated for between 7 and 18 h at the indicated temperatures, with the exception of the two highest-temperature points (80.6°C, and 90.3°C), for which the incubation time was 3 h and 4 h, respectively. Lamellar and Q_{II} phases coexisted in the range 55 to 57.4°C. The Q_{II} phase only was present in the range 58.3 to 64.6°C. The Q_{II} phase coexisted with the H_{II} phase at 80.6 and 90.3°C. The error bars represent the 95% confidence level uncertainty in the lattice constants, which were obtained by a linear regression fit to the d-spacings of the Q_{II} phase reflections.

obtained with samples incubated for periods ranging from 3 to 12 h at the temperatures indicated. The lattice parameters remained constant after the first few hours of incubation at each temperature and are assumed to represent equilibrium values. The figure shows that the unit cell of the Q_{II}-Pn3m phase undergoes a dramatic contraction with increasing temperature. In the interval from 55°C to 90°C, the lattice parameter decreases by a factor of almost three!

The Q_{II} Phases First Form with a Large, Non-Equilibrium Lattice Constant

The lattice constant of the Q_{II}-Pn3m phase first formed in either temperature ramp or jump experiments was larger than the equilibrium value at the same temperature. Thus, for example, when the Q_{II}-Pn3m phase forms at 59.6°C in the temperature ramp illustrated in Fig. 6*B*, the lattice constant is 331 Å, and decreases to 285 Å at 61.8°C. From Fig. 10, the equilibrium value at 61.8°C is only 188 Å. Likewise, when the Q_{II}-Pn3m phase first forms at 61.8°C in the temperature jump study reported on in Fig. 9*B*, its lattice constant is 209 Å, some 20 Å larger than the equilibrium value of 188 Å (Fig. 10). Similarly, the lattice constant of the Q_{II}-Im3m phase is initially large (348 Å) and decreases rapidly with time following a temperature jump (Fig. 9*B*).

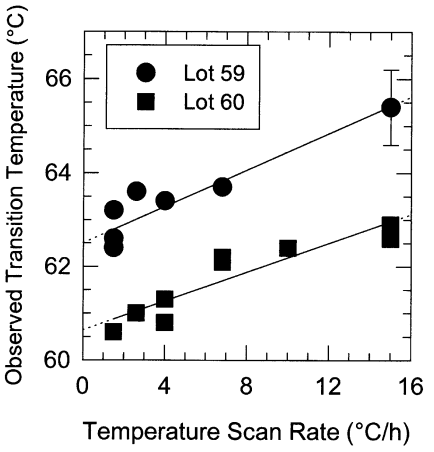

Fig. 11. Heating scan rate dependence of the phase transition temperature obtained by DSC on two different lots of DOPE-Me. All data points represent individual measurements, except for the datum for Lot 59 at 15°C/h, which shows the mean and standard deviation of seven trials. The lipid concentrations used in these experiments were between 15 and 33% (w/w) of DOPE-Me.

DSC and X-ray Diffraction Experiments on Different Lots of DOPE-Me

Different lots of DOPE-Me gave conflicting results in some of our diffraction experiments. Thus, for example at 58°C, the lag time for Q_{II} phase formation was 2.5 h with one lot and 16 h with another. DSC is a convenient method for quantifying phase behavior. The calorimeter used in this study facilitated direct comparisons between lipid lots by virtue of the fact that three samples and a reference could be run simultaneously (*see* Methods). Lots 59 and 60 were investigated most thoroughly. In both cases, TLC showed the lipid to be $>99.5\%$ pure.

Calorimetrically measured transition temperatures for lipids from Lots 59 and 60 are shown in Fig. 11. Clearly, there is a significant difference in the transition temperature between lots. While the transition temperature rises with scan rate, the lot-to-lot difference of approximately 2°C was insensitive to scan rate. In contrast to the transition temperature, the transition enthalpy averaged over all scan rates was not significantly different between lots (285 ± 25 cal/mole for Lot 59, 309 ± 13 cal/mole for Lot 60). The transition detected calorimetrically was probably of the L_α to H_{II} type. X-Ray diffraction measurements with Lot 59 lipid showed that the Q_{II} phase formed only after several hours of incubation at constant temperatures in the interval 59 to 62°C (*data not shown*). This suggests that the Q_{II} phase is unlikely to form on the time scale of the DSC experiments presented in Figure 11. However, the possibility that the transition measured at scan rates of <2°C/h might be of the L_α to Q_{II} type cannot be ruled out.

While the lot variability in transition temperature is significant, within a given lot the measured transition temperature is very reproducible. Thus, the T_H determined using six samples from Lot 63 was 63.7°C with a standard deviation of 0.4°C recorded at a scan rate of 1.5°C/h (Fig. 4). The origin of the lot-to-lot variability is not known. The purity of the MME used in the synthesis of DOPE-Me (Materials and Methods) does not seem to be an important factor. This was demonstrated by making TRXRD temperature-ramp measurements on DOPE-Me prepared with commercial grade MME (Lot 62) and with highly purified MME (Lot 63) (*see* Materials and Methods). Both had T_H values that were the same to within 0.5°C at a scan rate of 1.5°C/h (*data not shown*). This difference is not significant in light of the fact that the standard deviation on T_H is 0.4°C at the same scan rate. However, because of lot-to-lot variability of the type seen in Fig. 11, in the interests of uniformity all of the work reported on in this study was done with lipid from Lot 63, unless otherwise noted.

There was a clear scan-rate dependence to the transition temperature observed with both lots of lipid reported on in Fig. 11. Specifically, the transition temperature rose by about 3°C between 1.5°C/h and 15°C/h. Interestingly, this scan-rate dependence is remarkably similar to that seen for $T_{L/H}$ and T_H (Fig. 4), as will be discussed.

Discussion

Implications for the Mechanism of Lamellar/Non-Lamellar Phase Transitions in DOPE-Me

The lamellar/inverted phase transition mechanism proposed by Siegel (1999) rationalizes the relative rates of the L_α/Q_{II} and L_α/H_{II} phase transitions as a function of temperature in the context of a competition between the two transitions. The proposed mechanism is summarized in Fig. 12*A*. The first structure to form between two apposed L_α phase bilayers is a "stalk" connection between the facing monolayers of the apposed bilayers (Fig. 12*A2*). This expands into a trans-monolayer contact (TMC; Fig. 12*A3*), in which the distal monolayers of the two apposed bilayers pinch inwards to contact each other. The number of stalks and TMCs should increase with increasing temperature around T_H (Siegel, 1993, 1999) because the free energy of stalks and TMCs decreases as the absolute value of spontaneous curvature of the lipid increases, and this value rises with temperature. The TMC is postulated as an intermediate in the formation of *both* H_{II} and Q_{II} phases. The apparent competition between the Q_{II} and H_{II} phase formation rates is proposed to be due to the competition of the two processes for TMCs. If

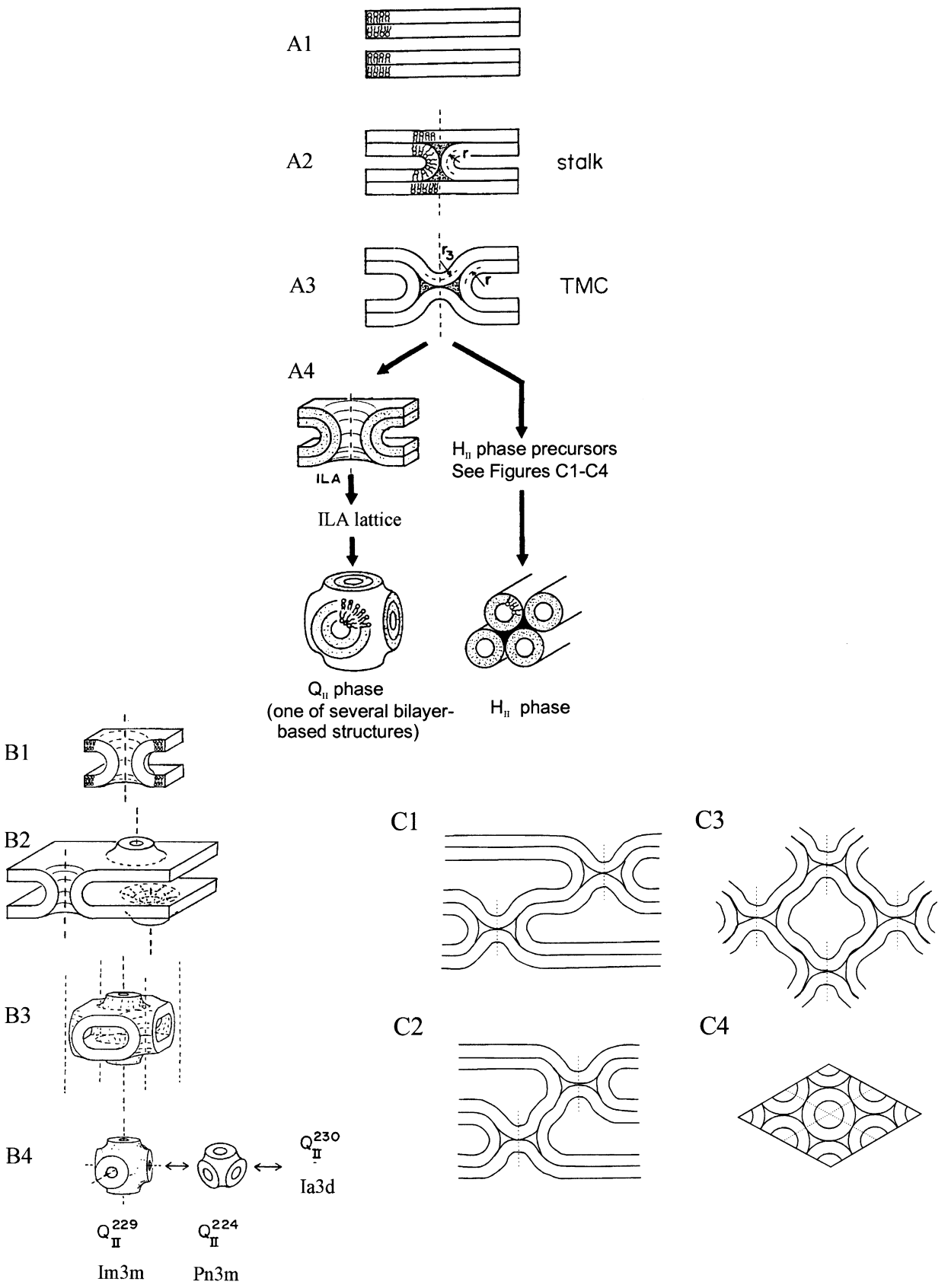

Fig. 12. A possible mechanism for lamellar/non-lamellar phase transitions in hydrated glycerophospholipids. In Parts *A* and *C*, slabs depict lipid monolayers. In Part *B*, slabs represent bilayers. *See* text for details. Adapted from Siegel and Banschbach (1990), Siegel and Epand, (1997), and Siegel (1999).

the bilayer diaphragm in the center of the TMC ruptures, the inner monolayers form continuous channels. This creates an interlamellar attachment (ILA; Fig. 12*A4*, *left*), which amounts to a catenoidal bilayer connection between the two original bilayers. Parenthetically, we note that this structure corresponds to a fusion pore between two liposomes. If enough ILAs form in the L_α phase, they can assemble into an ILA array, and subsequently form the bulk Q_{II} phase by a process outlined in Fig. 12*B* (Siegel & Banschbach, 1990). Briefly, as ILAs accumulate, a lattice develops that is made up of repeating units of the type shown in Fig. 12*B3*. The lattice has the same connectivity as the Q_{II}-Im3m phase (Fig. 12*B4*), which can transform to the Q_{II}-Im3m phase by bilayer bending. This transition should be facile because it does not require a change in bilayer connectivity (Andersson et al., 1988). On the other hand, the H_{II} phase can also assemble from TMCs (Fig. 12*A4*, *right*). A mechanism for H_{II} phase formation has been proposed and is shown in Fig. 12*C* (Siegel & Epand, 1997; Siegel, 1999). TMCs forming within a stack of L_α phase lamellae (seen in cross-section in Fig. 12*C1*) can reduce their energy (Siegel, 1999) by aggregating (Fig. 12*C2*). Aggregation reduces the TMC energy because it lessens the amount of curved bilayer skirt around the periphery of the two TMCs, which has an unfavorable curvature energy. If the aggregation process continues, eventually a body-centered or primitive tetragonal TMC lattice forms. A cross-section in the (110) plane of this lattice is shown in Fig. 12*C3*, and is compared to the cross-section of an H_{II} phase lattice in Fig. 12*C4*. The cross-section of the TMC lattice (Fig. 12*C3*) has the same overall symmetry as the H_{II} phase: hexagonally-packed closed monolayer cylinders. Thus, diffusion of lipid molecules into this structure from the contiguous L_α phase lamellae can rapidly extend the structure out of the plane of the paper to form domains of H_{II} phase (Fig. 12*C4*). The results of cryoelectron microscopy studies show that structures of the shape and size expected for TMCs and TMC aggregates form in dipalmitoleoyl phosphatidylethanolamine systems (Siegel & Epand, 1997). The model also predicts that ILAs should be thermodynamically more stable than the L_α phase over a broad temperature interval around T_H, which is consistent with the observed formation and persistence of ILAs over a temperature range extending from far below T_H to temperatures above T_H (*see* Siegel, 1999, and references therein).

This model qualitatively rationalizes the effect of temperature on the relative rates of Q_{II} and H_{II} phase formation (Fig. 6) as follows. First, Siegel (1999) showed that ILAs are thermodynamically stable at $T < T_H$. Thus, it is not surprising that the Q_{II} phase that forms from them is observed at temperatures below that where the H_{II} phase is stable ($T < 61$°C, Figs. 4 and 7). Second, once conditions have been adjusted so that the H_{II} phase can form, the rate of H_{II} phase formation should increase relative to Q_{II} phase formation as the temperature increases. This is supported by the data in Fig. 7, which shows that the rate of H_{II} phase formation is faster than Q_{II} phase formation at $T > 61$°C. This is because TMCs need only aggregate to form H_{II} precursors (Fig. 12*A4*, *right*), while individual TMCs must first form ILAs in order for the Q_{II} lattice to form (Fig. 12*A4*, *left*). Since the number of TMCs increases with temperature, the rate of aggregation of TMCs also increases rapidly, making H_{II} precursor formation more rapid relative to ILA formation as the temperature increases. Further, only a few TMC aggregates are necessary to transform the bulk of a sample from the L_α phase into the H_{II} phase, because H_{II} domains grow rapidly by diffusion once they are nucleated (Siegel, 1999). This probably explains why the H_{II} phase forms more quickly than the Q_{II} phase between 6l and 65°C, even though H_{II} phase disappears in favor of Q_{II} phase at longer times. In this temperature range, the Q_{II} phase is thermodynamically more stable than the H_{II} phase, but the Q_{II} phase simply is slow to form. The apparent kinetic competition between H_{II} and Q_{II} phase formation rates is consistent with the competition of the two processes for a common intermediate structure (TMC). We speculate that the slow (hours) disappearance of the H_{II} phase at 61–65°C occurs via either an equilibration of the H_{II} phase with TMC aggregates and TMCs, which can convert to ILAs and Q_{II} phases, or via some direct H_{II}/Q_{II} transition mechanism. Third, in samples jumped to high temperatures (67°C, for example), the Q_{II} phase appears in short order after the H_{II} phase. Thus, for example, the H_{II} phase forms within 1 min at 67°C, with the Q_{II} phase appearing some 8 min later (Fig. 7). The increase in Q_{II} phase formation rate with increasing temperature may be due to rapid consumption of the L_α phase by growing H_{II} domains under these conditions. Some ILAs probably appear at the start of the incubation under these conditions. Rapid consumption of the L_α phase will tend to concentrate the ILAs into a small region of the sample where they can form Q_{II} lattices more rapidly than at 60.7–61.7°C. In samples jumped to very high temperatures (80.6 and 90.3°C, for example), Q_{II} phase formation takes much longer (hours; data not shown). It may be that under these conditions the initial H_{II} phase formation is so rapid and complete that very few ILAs have time to form, so that the Q_{II} phase forms directly from the H_{II} phase by some other, slower process. Taken together, the qualitative predictions of the

model are in good agreement with the observed transition kinetics in this system.

DOPE-Me Phase Behavior and Phase Transition Kinetics

The equilibrium values of T_Q and T_H in hydrated DOPE-Me have proved difficult to determine with great certainty for several reasons. We begin the discussion by focusing on T_Q. The L_α/Q_{II} transition in DOPE-Me is notoriously hysteretic (e.g., Gagné et al., 1985; Gruner et al., 1988; Ellens et al., 1989) so that an equilibrium value of T_Q cannot be obtained in the cooling direction. The heating direction has its own problems, as illustrated in the current study. Thus, the value of T_Q (determined in the heating direction) seems to change non-linearly as zero scan rate is approached. Formal extrapolation of T_Q to zero rate gives a T_Q of ~58°C (Fig. 4). However, the temperature-jump data in Fig. 7*A* show that the Q_{II} phase can form after 6 h of incubation at 55°C. These same data suggest further that the value of T_Q may be limited, to some degree, by the time one is prepared to wait for the Q_{II} phase to appear. Regardless, the temperature-jump data show clearly that the Q_{II} phases can form and are stable at temperatures between 55°C and at least 90.3°C.

For the L_α/H_{II} transition, the value of $T_{L/H}$ extrapolated to zero scan rate is ~63.8°C (Fig. 4). However, temperature-jump data show that although the H_{II} phase can form at this temperature, it is the Q_{II} phase that represents the equilibrium state in the interval between 61 and 65°C (Fig. 5).

The tardiness of Q_{II} and H_{II} phase formation below 64°C (Fig. 7) explains why the Q_{II} and H_{II} phases appeared at higher temperatures in temperature ramp (Fig. 4) than in temperature jump experiments (Fig. 7). In the former, even the slowest scan rate used (0.75°C/h) was fast enough such that the temperature of the sample increased substantially before the phase had time to form. This amounted to several hours at the lowest temperatures used (Fig. 7). Together, the temperature ramp and jump data show that there is a direct L_α/Q_{II} phase transition in samples incubated at constant temperature between approximately 55 and 60°C, or in samples ramped through the interval 55 to 63°C at rates <2°C/h (Fig. 5). The H_{II} phase forms at higher temperatures in both types of experiments. The Q_{II} phase is only sometimes observed in the temperature interval up to 70°C at scan rates above 3°C/h.

The fact that the H_{II} phase can form more rapidly than the Q_{II} phase, and that it can then disappear in favor of the Q_{II} phase (in jump experiments to temperatures between 61 and 65°C) has important implications. It suggests that the phase that forms most rapidly under these circumstances is determined partly by the competing rates of the L_α/Q_{II} and L_α/H_{II} transitions, and not solely by the relative thermodynamic stability of the two non-lamellar phases, as already discussed.

The current study forms the basis for a separate investigation concerned with the mechanism of fusion in a model membrane consisting of hydrated DOPE-Me (Siegel et al., in preparation). In the latter study, transmembrane peptides were to be combined with hydrated lipid co-dissolved in TFE. In due course, the TFE is removed. Nonetheless, given the sensitivity of the system's phase behavior as detailed above, it was important to determine ahead of time if the TFE approach would influence phase behavior in any way. The data in Fig. 4 show convincingly that TFE had no significant impact on the relevant L_α/Q_{II} and L_α/H_{II} phase transitions.

The data in Fig. 4 also show that temperature-ramp experiments performed at a rate of 1.5°C/h yield the same T_Q value, to within about 1°C or less, as those done at lower scan rates. A scan rate of 1.5°C/h is therefore slow enough to ensure that a direct L_α/Q_{II} transition occurs in DOPE-Me, but is still fast enough to allow for the collection of data on a time scale that satisfies the limitations of our experimental tools. The latter include image decay on phosphor image plate detectors and synchrotron beam time. Accordingly, this same temperature scan rate was implemented in the study of transmembrane peptide effects on the T_Q of DOPE-Me (Siegel et al., in preparation).

Comparison with Previous Observations of DOPE-Me Phase Behavior

Siegel & Banschbach (1990) first showed that the Q_{II} phase forms during slow heating scans of hydrated DOPE-Me. The current work extends these results by establishing the kinetics of Q_{II} and H_{II} phase formation in temperature jump and temperature ramp experiments, and by showing that the onset temperatures for Q_{II} and H_{II} phase formation are both scan rate-dependent, that the rates of Q_{II} and H_{II} phase formation compete in a temperature interval above T_Q, and that lot-to-lot differences in DOPE-Me can affect phase transition kinetics and transition temperatures. However, some of the results in Siegel and Banschbach (1990) are consistent with those of the current study as follows. Siegel and Banschbach (1990) reported that a direct L_α/Q_{II} phase transition is not observed in temperature ramps unless the scan rate is reduced to ca 1°C/h, in agreement with the data in Fig. 4. They also reported that the midpoint of the L_α/Q_{II} phase transition in DSC experiments at 1.1°C/h was 61.3 ± 0.9°C, and that the Q_{II} phase was observed by x-ray diffraction at 61.0°C, but not at 59.6°C. Our data show that the onset temperature for Q_{II} phase formation is 55°C, although

long incubation times were required to observe it (Fig. 7*A*).

We suspect that the lower T_Q values in the current study are due to the greater sensitivity of our x-ray measurements and to the width of the L_α/Q_{II} phase transition (ca 4°C at a scan rate of 1.5°C/h). Thus, for example, Siegel and Banschbach (1990) used exposures of 3 h to produce good diffraction patterns of Q_{II} phase samples. In contrast, our rotating-anode apparatus required exposures of 30 min or less, and the synchrotron experiments produced excellent diffraction data in 1 min. Siegel and Banschbach (1990) also inferred the presence of a Q_{II}/H_{II} phase transition at 72 to 79°C from DSC data, but did not identify the phases involved. In contrast, our data show that the Q_{II}-Pn3m phase does not disappear but coexists with the H_{II} phase at 80.6 and 90.3°C. We do not know the reason for this discrepancy.

In contrast to the results of the current study, Colotto et al. (1996) and Colotto and Epand (1997) reported that hydrated DOPE-Me did not form a Q_{II} phase when heated in a step-wise fashion through the temperature interval of 60 to 80°C. These results however, may be consistent with ours when compared on the same time scale. We have shown that heating in single steps (corresponding to temperature jumps) in the vicinity of 60°C can produce the H_H phase initially, while the Q_{II} phase forms after some time (Figs. 5*B* and 7). Colotto et al. (1996) and Colotto and Epand (1997) integrated diffraction data for only 5–15 min after 5 min of equilibration at the experimental temperature. We have found that it can take an hour or more for Q_{II} phases to develop after temperature jumps in this range (Fig. 7*A*), although intense H_{II} phase reflections appear quickly (Figs. 7*B* and 9*A*). In samples subjected to a succession of temperature steps between 60 and 80°C, it could be that the Q_{II} phase would not have time to form in detectable amounts at the lower temperatures, and that H_{II} phase formation would dominate at the higher temperatures. Thus, it makes sense that the H_{II}, and not the Q_{II} phase, was observed in the protocol of Colotto et al. (1996) and Colotto and Epand (1997). Moreover, the x-ray apparatus used in the latter two studies was not capable of detecting the small-angle reflections (large interplanar spacings) that are generated by nascent Q_{II} phases at temperatures near 60°C (Fig. 9*B*). The maximum interplanar spacing their apparatus could detect was 110 Å (R. M. Epand, personal communication). Our results show that the first Q_{II} reflections to appear correspond to interplanar spacings of more than 125 Å (q = ca 0.05 $Å^{-1}$ or less, Fig. 8).

Lot-to-Lot Variability in Phase Behavior of DOPE-Me

In this study we have shown that there are significant differences in the behavior of different lots of DOPE-Me as received from the manufacturer. The reasons for the inter-lot variability are unclear. The kinetics of Q_{II} and H_{II} phase formation appear to be finely balanced around 60°C in DOPE-Me. It is possible that very low levels of impurities (lipid or inorganic salts) have substantial effects on the rates of H_{II} and Q_{II} phase formation. There is precedent for this. Tenchov, Koynova & Rapp (1994) found that adding salts or disaccharides to the aqueous phase greatly accelerates Q_{II} phase formation during temperature-cycling in dielaidoylphosphatidylethanolamine. DOPE-Me has been used extensively in studies linking Q_{II} phase formation with membrane fusion. It is important for researchers to control for these lot-to-lot differences, or to limit studies to a single lot.

Conclusions

The study shows that the rates of appearance of the Q_{II} and H_{II} phases in hydrated DOPE-Me lamellae are temperature-sensitive, with a direct L_α/Q_{II} phase transition occurring either at temperature scan rates <2°C/h or during long incubations at temperatures between approximately 55 and 60°C. The results are consistent with a recently proposed lamellar/non-lamellar phase transition mechanism in glycerophospholipids (Siegel, 1999). The study establishes a basis for examining the effects of fusion peptides on the temperature and kinetics of the L_α/Q_{II} and L_α/H_{II} phase transitions in DOPE-Me.

We are very grateful for the expert assistance of Dr. Malcolm S. Capel (National Synchrotron Light Source, Beamline X12B) in collecting the synchrotron TRXRD data. This project was supported by grants from the NIH (GM56969, GM61070) and the NSF (DIR 9016689, DBI 9981990).

References

Andersson, S., Hyde, S.T., Larsson, K., Lidin, S. 1988. Minimal surfaces and structures: From inorganic and metal crystals to cell membranes and bioploymers. *Chem. Reviews* **88:**221–242

Basañes, G., Gõni, F.M., Alonso, A. 1998. Effect of single chain lipids on phospholipase C-promoted membrane fusion. A test for the stalk hypothesis of membrane fusion. *Biochemistry* **37:** 3901–3908

Blanton, T.N., Huang, T.C., Toroya, H., Hubbard, C.R, Robie, S.B., Louer, D., Gobel, H.E., Will, G., Gilles, R., Rafferty, T. 1995. JCPDS — International centre for diffraction data study of silver behenate. A possible low-angle X-ray diffraction calibration standard. *Powder Diffraction* **10:**91–95

Capel, M.S., Smith, G.C., Yu, B. 1995. One- and two-dimensional x-ray detector systems at NSLS beam-line X12B, for time-resolved and static x-ray diffraction studies. *Rev. Sci. Instruments* **66:**2295–2299

Cheng, A., Caffrey, M. 1996. Free radical mediated x-ray damage of model membranes. *Biophys. J.* **70:**2212–2222

Cherezov, V., Riedl, K.M., Caffrey, M. 2002. Too hot to handle? Synchrotron x-ray damage of lipid membranes and mesophases. *J. Synchrotron Radiation* **9:**333–341

Colotto, A., Martin, I., Ruysschaert, J.-M., Sen, A., Hui, S.W., Epand, R.M. 1996. Structural study of the interaction between the SIV fusion peptide and model membranes. *Biochemistry* **35:**980–989

Colotto, A., Epand, R.M. 1997. Structural study of the relationship between the rate of membrane fusion and the ability of the fusion peptide of influenza virus to perturb bilayers. *Biochemistry* **36:**7644–7651

Darkes, M.J.M., Harroun, T.A., Davies, S.M.A., Bradshaw, J.P. 2002. The effect of fusion inhibitors on the phase behaviour of N-methylated dioleoylphosphatidylethanolamine. *Biochim. Biophys. Acta* **1561:**119–128

Davies, S.M.A., Epand, R.F., Bradshaw, J.P., Epand, R.M. 1998. Modulation of lipid polymorphism by the feline leukemia virus fusion peptide: Implications for the fusion mechanism. *Biochemistry* **37:**5720–5729

Ellens, H., Siegel, D.P., Alford, D., Yeagle, P.L., Boni, L., Lis, L.J., Quinn, P.J., Bentz, J. 1989. Membrane fusion and inverted phases. *Biochemistry* **28:**3692–3703

Ellington, J.S., Lands, W.E.M. 1968. Phospholipid reactivation of plasmalogen metabolism. *Lipids* **3:**111–120

Epand, R.M., Epand, R.F. 1994. Relationship between the infectivity of influenza virus and the ability of its fusion peptide to perturb bilayers. *Biochem. Biophys. Res. Commun.* **202:**1420–1425

Epand, R.F., Martin, I, Ruysschaert, J.-M., Epand, R.M. 1994. Membrane orientation of the SIV fusion peptide determines its effect on bilayer stability and ability to promote membrane fusion. *Biochem. Biophys. Res. Commun.* **205:**1938–1943

Gagné, J., Stamatatos, L., Diacovo, T.S., Hui, W., Yeagle, P.L., Silvius, J.R. 1985. Physical properties and surface interactions of bilayer membranes containing N-methylated phosphatidylethanolamines. *Biochemistry* **24:**4400–4408

Gruner, S.M., Tate, M.W., Kirk, G.L., So, P.T.C., Turner, D.C., Keane, D.T., Tilcock, C.P.S., Cullis, P.R. 1988. X-Ray Diffraction study of the polymorphic behaviour of N-methylated dioleoylphosphatidylethanolamine. *Biochemistry* **27:**2853–2866

Hammersley, A.P., Svensson, S.O., Hanfland, M., Fitch, A.N., Hausermann, D. 1996. Two-dimensional detector software: from real detector to idealised image or two-theta scan. *High Pressure Research* **14:**235–248

Hammersley, A.P. 1997. FIT2D: An introduction and overview. ESRF Internal Report, ESRF97HA02T

Hyde, S., Andersson, S., Ericsson, B., Larsson, K. 1984. A cubic structure consisting of a lipid bilayer forming an infinite periodic minimum surface of the gyroid type in the glyceromonooleate-water system. Z. *Krystallogr.* **168:**213–219

Kates, M., Sastry, P.S. 1969. Phospholipase D. *Methods in Enzymology* **14:**173–181

Killian, J.A., Salemink, I., de Planque, M.R.R., Lindblom, G., Koeppe II, R.E., Greathouse, D.V. 1996. Induction of nonbilayer structures in diacylphosphatidylcholine model membranes by transmembrane α-helical peptides: Importance of hydrophobic mismatch and proposed role of tryptophans. *Biochemistry* **35:**1037–1045

Koynova, R., Caffrey, M. 1998. Phases and phase transitions of the phosphatidylcholines. *Biochim. Biophys. Acta* **1376:**91–145

Nieva, J.L., Alonso, A., Basáñes, G., Goni, F.M., Gulik, A., Vargas, R., Luzzati, V. 1995. Topological properties of two cubic phases of a phospholipid:cholesterol:diacylglycerol aqueous system and their possible implications in the phospholipase C-induced liposome fusion. *FEBS Letters* **368:**143–147

Siegel, D.P. 1993. Energetics of intermediates in membrane fusion: Comparison of stalk and inverted micellar intermediate mechanisms. *Biophys. J.* **65:**2124–2140

Siegel, D.P. 1999. The modified stalk mechanism of lamellar/inverted phase transitions and its implications for membrane fusion. *Biophys. J.* **76:**291–313

Siegel, D.P., Banschbach, J.L. 1990. Lamellar/inverted cubic (L_α/Q_{II}) phase transition in N-methylated dioleoylphosphatidylethanolamine. *Biochemistry* **29:**5975–5981

Siegel, D.P., Banschbach, J., Alford, D., Ellens, H., Lis, L.J., Quinn, P.J., Yeagle, P.L., Bentz J. 1989a. Physiological levels of diacylglycerols in phospholipid membranes induce membrane fusion and stabilize inverted phases. *Biochemistry* **28:**3703–3709

Siegel, D.P., Burns, J.L., Chestnut, M.H., Talmon, Y. 1989b. Intermediates in membrane fusion and bilayer/nonbilayer phase transitions imaged by time-resolved cryo-transmission electron microscopy. *Biophys. J.* **56:**161–169

Siegel, D.P, Epand, R.M. 1997. The mechanism of lamellar-to-inverted hexagonal phase transitions in phosphatidylethanolamine: Implications for membrane fusion mechanisms. *Biophys. J.* **73:**3089–3111

Siegel, D.P, Green, W.J, Talmon, Y. 1994. The mechanism of lamellar-to-inverted hexagonal phase transitions: A study using temperature-jump cryo-electron microscopy. *Biophys. J.* **66:**402–414

Skipski, V.P., Peterson, R.F., Barclay, M. 1968. Separation of phosphatidylethanolamine, phosphatidylserine, and other phospholipids by thin-layer chromatography. *J. LipidRes.* **3:**467–475

Tenchov, B, Koynova, R., Rapp, G. 1998. Accelerated formation of cubic phases in phosphatidylethanolamine dispersions. *Biophys. J.* **75:**853–866

Yeagle, P.L., Epand, R.M., Richardson, C.D., Flanagan, T.D. 1991. Effects of the 'fusion peptide' from measles virus on the structure of N-methyl dioleoylphosphatidylethanolamine membranes and their fusion with Sendai virus. *Biochim. Biophys. Acta* **1065:**49–53

Zhu, T., Caffrey, M. 1993. Thermodynamic, thermomechanical and structural properties of a hydrated asymmetric phosphatidylcholine. *Biophys. J.* **65:**939–954